Neuron, Volume *81*

Supplemental Information

The Projective Field of Retinal Bipolar Cells and Its Modulation by Visual Context

Hiroki Asari and Markus Meister

Inventory of supplemental information

- Supplemental data:
  - Figure S1, related to Figure 3.
  - Figure S2, related to Figure 4.
  - Figures S3 and S4, related to Figures 5 and 6.
  - Figure S5, related to Figure 7.
- Supplemental experimental procedures.
- Supplemental references.

Supplemental data

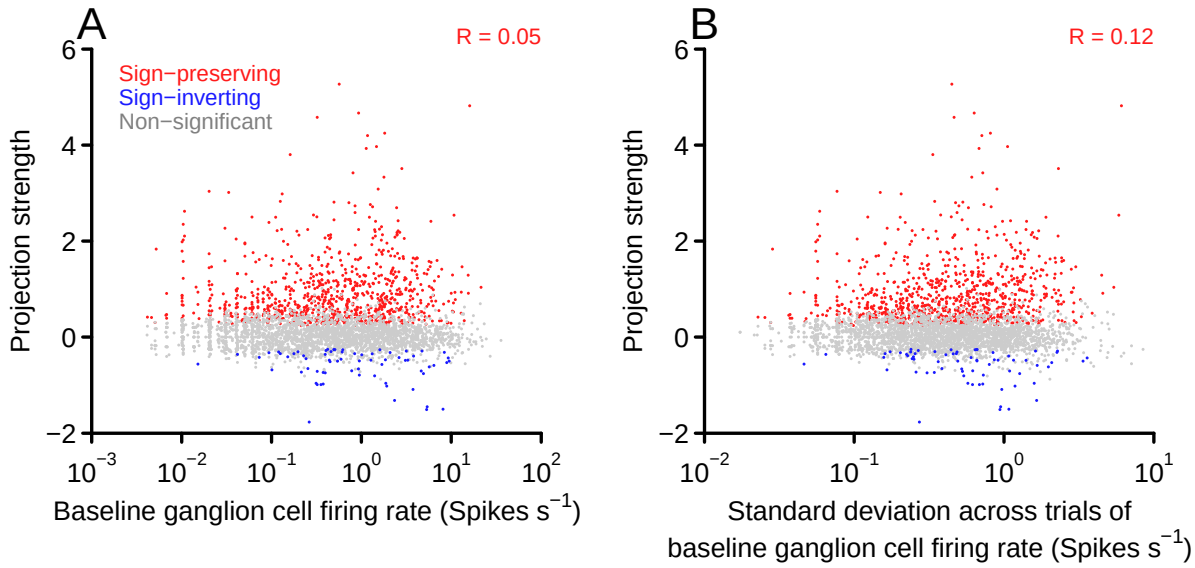

Figure S1: Projection strength is not correlated with the baseline firing rate of ganglion cells or its variability across trials, related to Figure 3.

The projection strength is defined as a ratio of evoked changes in firing rate, normalized by unrelated changes in the firing rate (Eq.(2)). Here we test whether the resulting ratio is systematically influenced by the normalization factor.

(A) Population data of the projection strength (red, significant sign-preserving; blue, significant sign-inverting; gray, non-significant) as a function of the baseline firing rate of ganglion cells. Correlation coefficient for sign-preserving projections (R) is displayed on the top-right corner.

(B) Population data of the projection strength as a function of the variability of baseline ganglion cell firing rate, measured as the standard deviation across trials (displayed as in panel A).

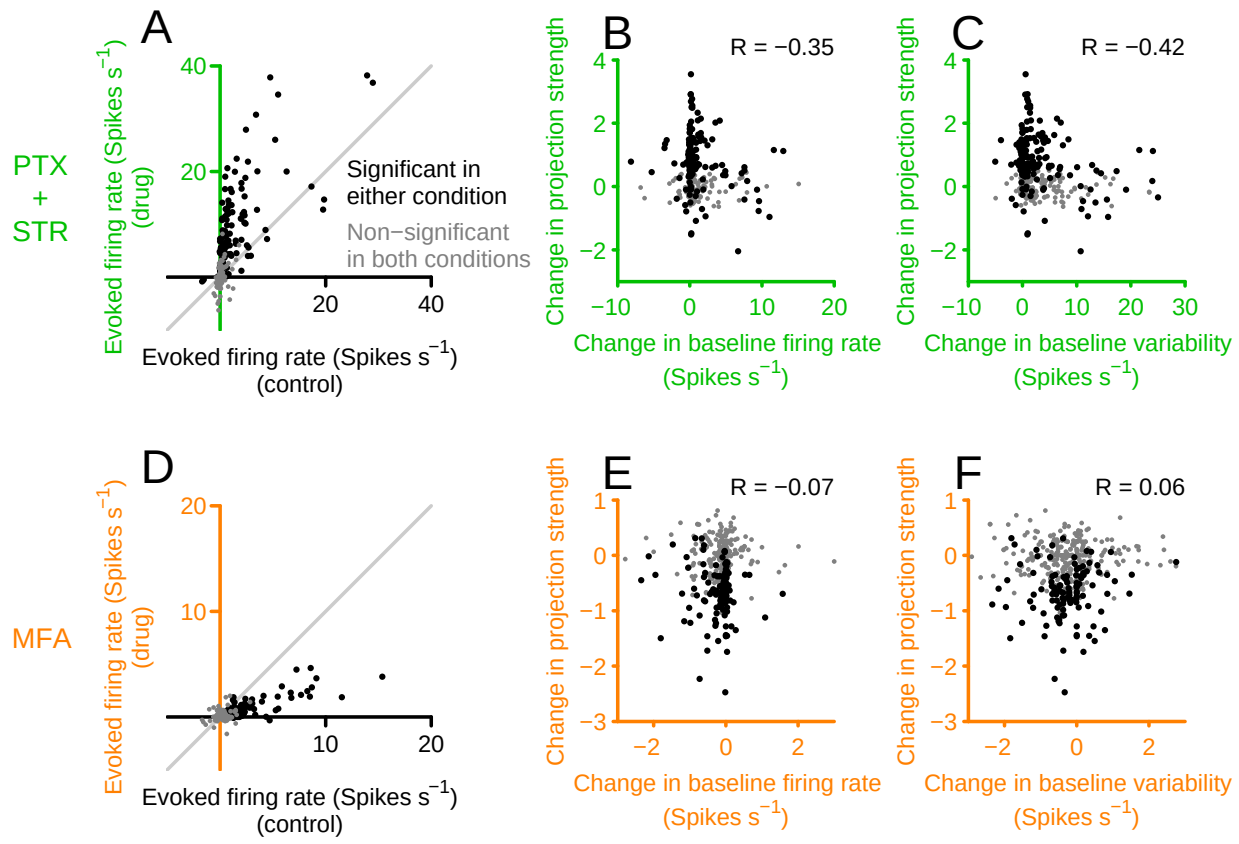

Figure S2: Change in projection strength by drug application is not correlated with change in baseline ganglion cell firing rate or its variability across trials, related to Figure 4.

(A, D) Net evoked firing rate of ganglion cells in response to bipolar cell current injections before and after applying picrotoxin and strychnine (A; PTX+STR) or meclofenamic acid (D; MFA): black, significant projection in at least one condition; gray, non-significant in both conditions. Displayed as in Figures 4A and 4D, respectively.

(B, C, E, F) Change in bipolar cell projection strength by the drug application (B, C: picrotoxin and strychnine; E, F: meclofenamic acid) as a function of the changes in baseline ganglion cell firing rate (B, E) or its variability, measured as the standard deviation across trials (C, F). Correlation coefficient for significant projections (R) is displayed on the top-right corner of each panel.

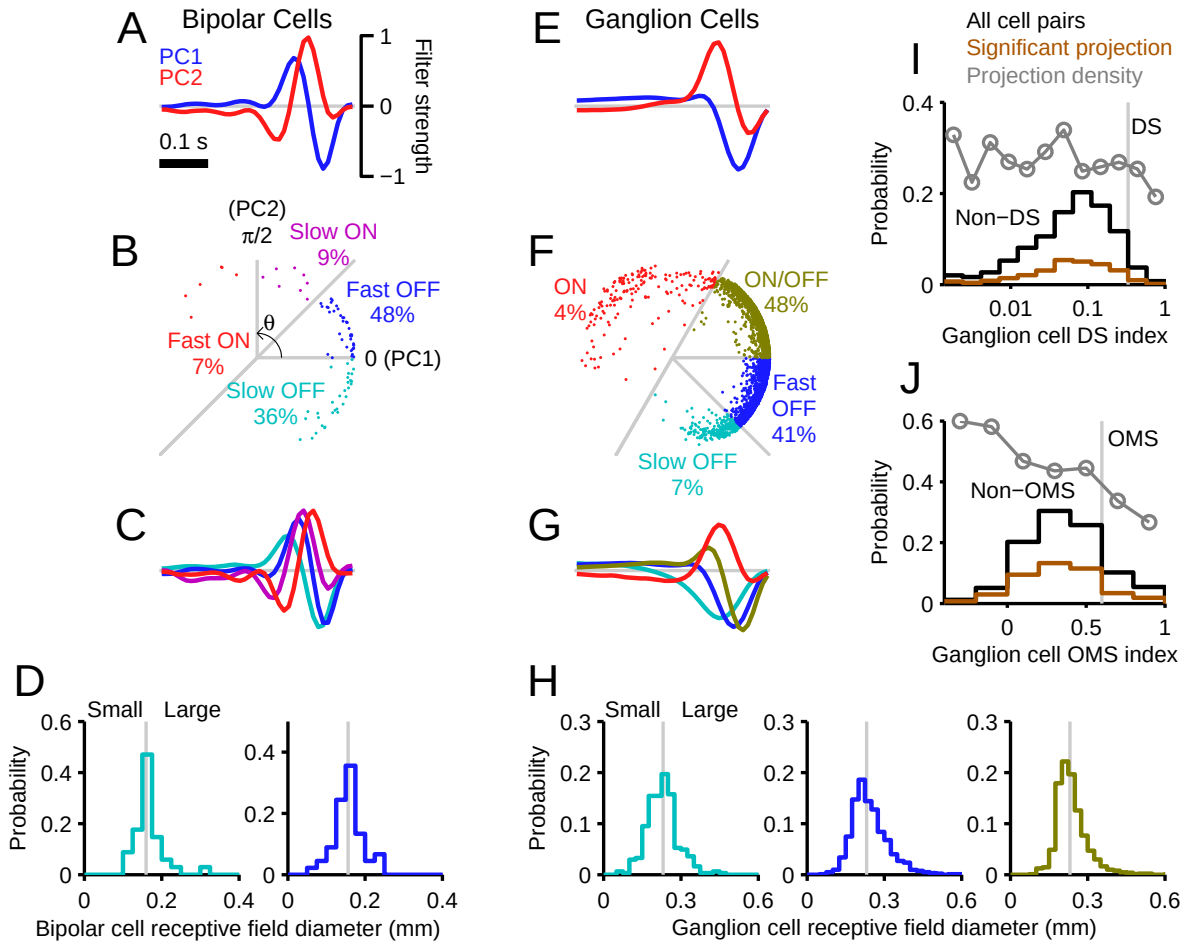

Figure S3: Cell type classification, related to Figures 5 and 6.

(A–D) To physiologically classify bipolar cell types, we performed principal component analysis on their temporal filters (A) and projected them onto the two-dimensional space spanned by the first two principal components (PC1 and PC2; $N = 86$ cells; B). Based on the angle θ around the origin in this space (0, PC1; $\pi/2$, PC2; boundaries in gray lines; B), we grouped the temporal filters into four subtypes (mean filters color-coded in panel C; same scale as in panel A). The Slow OFF (cyan) and Fast OFF (blue) cell types were further divided into Small and Large types based on the receptive field diameters (D; boundary in gray at the median).

(E–H) Ganglion cells were classified by the same methods into four subtypes from the temporal filters ($N = 4{,}236$ cells; E–G) with a finer subdivision by the receptive field size (except for the ON cell type; H). Displayed as in panels A–D.

(I) Ganglion cell direction selectivity (DS) index was calculated from the spatiotemporal receptive field by Fourier analysis (from Eq.(S1); black, all data; brown, significant projection) for classifying DS and Non-DS cells (boundary in gray vertical line). Bipolar cell projection density (gray) was not dependent on the DS index (slope, -0.02 ± 0.03; y-intercept, 0.24 ± 0.05; linear regression with 95% confidence interval).

(J) Object motion sensitivity (OMS) index was calculated for a subset of ganglion cells (within 0.35 mm from target bipolar cells; $N = 845$) from their responses to a grating stimulus with global and differential motion between center region (1-mm-diameter circular area centered at the target bipolar cells) and the surround region (Eq.(S2)). Bipolar cell projection was observed less frequently to OMS ganglion cells (slope, -0.27 ± 0.07; y-intercept, 0.53 ± 0.04). Displayed as in panel I.

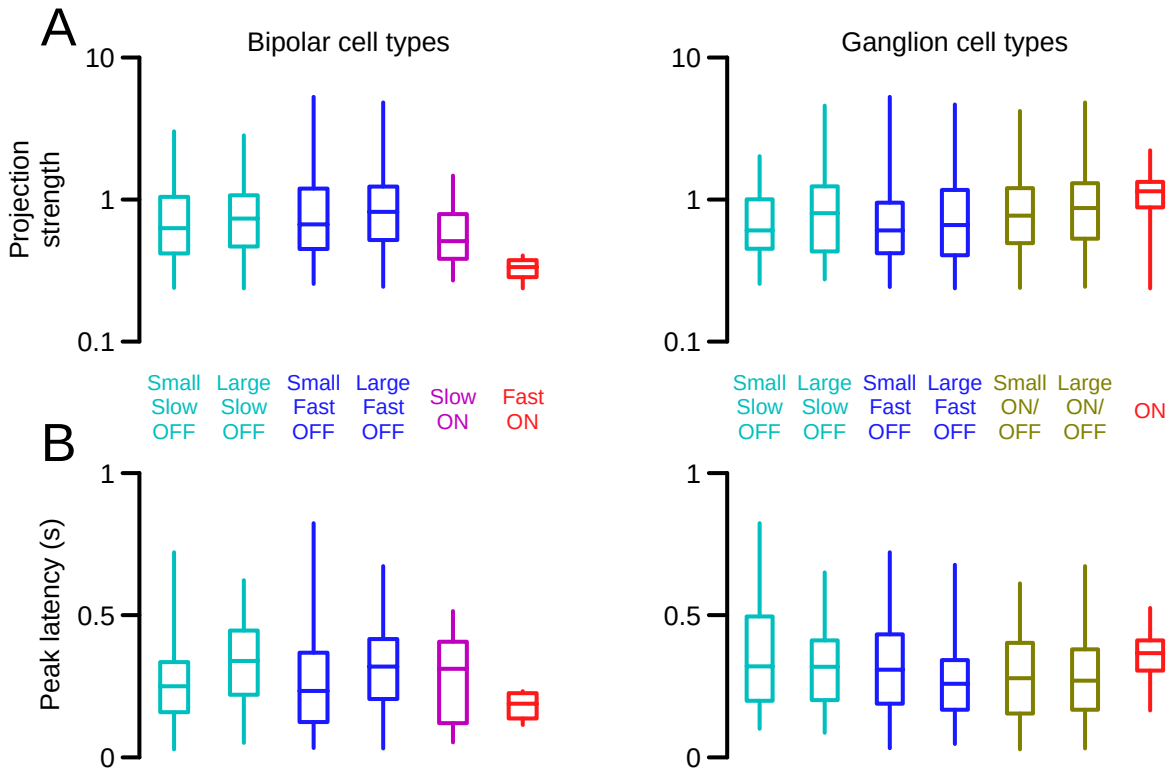

Figure S4: Projection strength and peak latency across different cell types, related to Figures 5 and 6.

(A) Projection strength across different cell types. The data were sorted by projections from distinct bipolar cell types (left), or by projections to distinct ganglion cell types (right). The box plot represents the minimum, first quartile, median, third quartile, and maximum values of the projection strength for the cell pairs with significant sign-preserving projection in each category. Note logarithmic axis.

(B) Peak latency of ganglion cell responses to bipolar cell depolarization (left, across bipolar cell types; right, across ganglion cell types; displayed as in panel A).

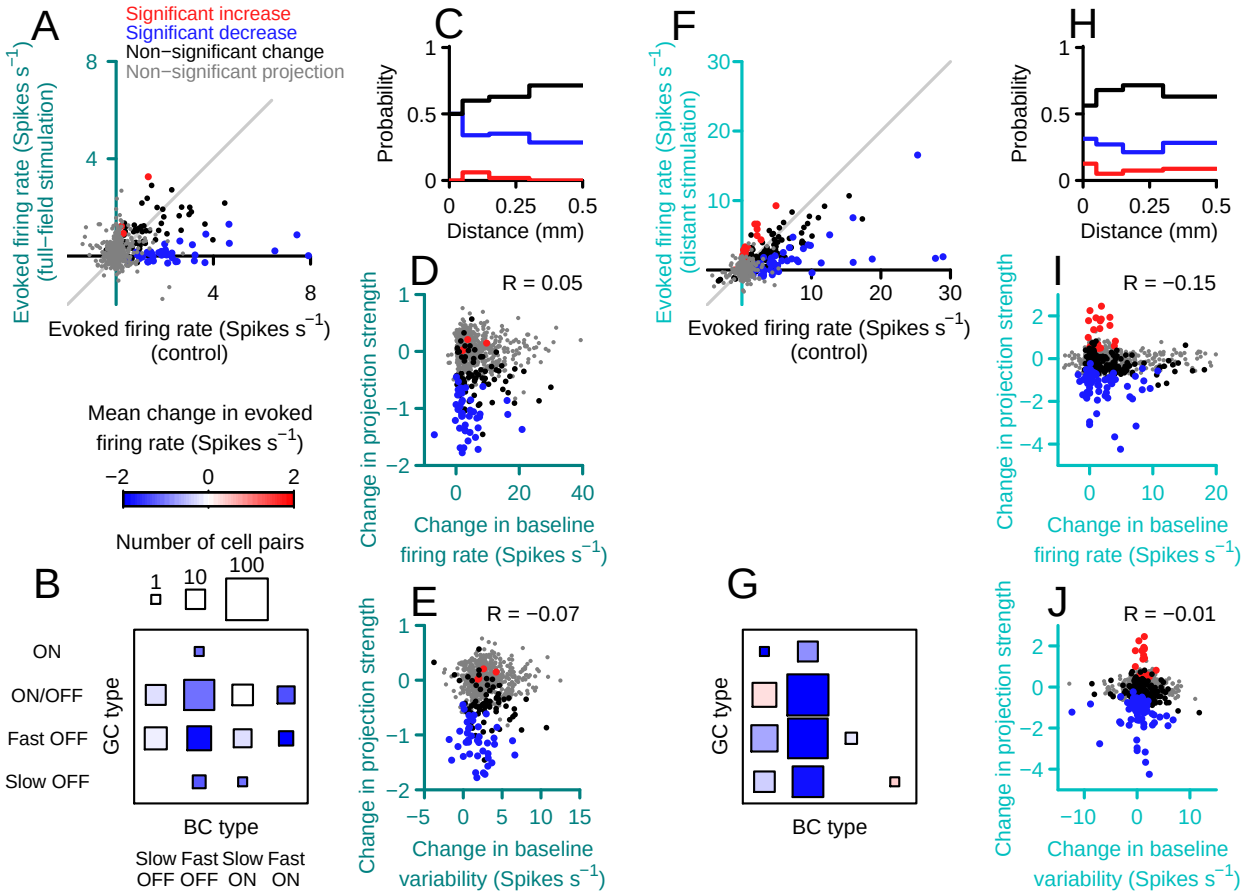

Figure S5: Change in projection strength by visual stimulation is not correlated with change in baseline ganglion cell firing rate or its variability across trials, related to Figure 7.

(A) Net evoked firing rate of ganglion cells by bipolar cell current injection in the presence and absence of full-field visual stimulation (gray, non-significant projection in both conditions; black, red, and blue, significant projection in at least one condition; red, significant increase during visual stimulation; blue, significant decrease). Displayed as in Figure 7A.

(B) Mean change in the net evoked firing rate among distinct pairs of bipolar and ganglion cell types (red hue, positive; blue hue, negative; displayed as in Figure 7D).

(C) Fraction of cell pairs with significant projection that showed significant increase (red) or decrease (blue) in the projection strength by the visual stimulation (black, non-significant change), plotted against the distance between the cells.

(D, E) Change in bipolar cell projection strength by the full-field visual stimulation as a function of the changes in baseline ganglion cell firing rate (D) or its variability, measured as the standard deviation across trials (E). Correlation coefficient for significant projections (R) is displayed on the top-right corner of each panel.

(F–J) Same analysis for the effects of distant visual stimulation (displayed as in panels A–E, respectively).

Supplemental experimental procedures

Electrophysiology

The dark-adapted retina of a larval tiger salamander (*Ambystoma tigrinum*) was isolated and placed on a flat array of 61 extracellular electrodes with the ganglion cell side down (Meister et al., 1994). The retina was superfused with oxygenated Ringer's medium (in mM: NaCl, 110; $NaHCO_3$, 22; KCl, 2.5; $MgCl_2$, 1.6; $CaCl_2$, 1; and D-glucose, 10; equilibrated with 95% O_2 and 5% CO_2 gas) at room temperature. Sharp intracellular microelectrodes were filled with 2 M potassium acetate and 3% Rhodamine Dextran 10,000 MW (fluorescent dye; Molecular Probes) with a final impedance of 150-250 MΩ, and blindly inserted into various cells until one with the visual response characteristics matching those of bipolar cells or amacrine cells was found (Baccus and Meister, 2002). We used an Axoclamp 2B amplifier (Molecular Devices) in bridge mode to monitor membrane potential and deliver command signals into individual cells. Specifically, we alternately delivered depolarizing and hyperpolarizing square pulse currents (500 pA; 1 s each) into cells with 2 s intervals (see Figure 1). Depolarization of the bipolar cell by the current injection was not significantly different among the bipolar cell types (ON, 29.4 ± 5.6 mV; OFF, 40.5 ± 4.5 mV; mean $\pm$ standard error; $p > 0.39$, rank sum test). To test whether this current injection somehow depolarizes ganglion cells directly, we injected current into the extracellular space between neurons and found no resulting activity in ganglion cells. Furthermore, current injection into amacrine cells was found to inhibit ganglion cells (Figures 2B and 3E). For additional control experiments, see Asari and Meister (2012).

In total, recordings were made from 86 bipolar cells together with 4,236 ganglion cells, and from 10 amacrine cells with 347 ganglion cells. To study interactions with the surrounding circuits, 10 bipolar cells were examined with 100 μM picrotoxin and 1.0 μM strychnine, and 8 bipolar cells with 100 μM meclofenamic acid (Figures 4 and S2). These drugs were also applied during 5 amacrine cell recordings (Figure 4B and E). Because washout of these drugs from a whole-mount preparation is slow (Cook et al., 2000; Veruki and Hartveit, 2009), we could not achieve full reversal of the drug effects within the available time—typically, half an hour for the intracellular recordings. Thus we only compared measurements before and after drug application, with no analysis of the washout. To study visual context-dependence of bipolar cell projective fields, 27 bipolar cells were examined in the presence of distant visual stimuli, and 15 bipolar cells under full-field visual stimulation (Figures 7 and S5).

Visual stimulation

Visual stimuli were displayed on a gamma-corrected cathode-ray tube monitor (DELL E773c; frame rate 100 Hz; mean luminance 18 mW/m^2) and projected onto the photoreceptor layer of the retina. We used the following four sets of visual stimuli, although not all stimuli were presented to all cells.

1. To identify the cells penetrated by the sharp electrodes, we examined their responses to a flashing center spot (200 μm diameter), annulus ring (500 μm inner diameter; 1,000 μm outer diameter), or uniform field.

2. To map the spatio-temporal receptive fields of all recorded cells (see Figure 1A–D for example), we presented randomly flickering checkerboard stimuli for 10-15 minutes (20-100 μm square fields; Meister et al., 1994).

3. To examine the visual context-dependence of bipolar cell projective fields (Figures 7 and S5), we presented full-field random flicker (100 frames per second; intensity drawn from Gaussian distribution with mean luminance of 18 mW/m^2 and standard deviation of 7 mW/m^2) while injecting current into the target bipolar cell.

4. To examine interactions between a bipolar cell and its surrounding circuitry (Figures 7 and S5), we covered the entire visual field (6,400$\times$4,800 μm) with a grating of black and white stripes (80 μm width), and divided it into a circular center region (1,000 μm in diameter, centered at the bipolar cell soma) and the surrounding background region. In combination with the current injection into the bipolar cell, the surrounding grating was then either shifted by a half period every 200 ms or jittered on every 10 ms frame update (Gaussian random motion with a standard deviation of 2 mm$/$s, corresponding to a step size of 2 pixels$/$frame) to recruit inputs from wide-field amacrine cells (Baccus et al., 2008; Geffen et al., 2007). In the former shifting case, every current injection trial was delayed by 50 ms to vary the relative timing between the onset of square pulse currents and that of background stimulus motion. The center region remained static so as not to visually stimulate the current-stimulated bipolar cell or nearby ganglion cells (Asari and Meister, 2012). To examine object motion sensitivity of ganglion cells (Figures 5E and 6D), these center and surround regions were shifted in sync or out of sync at 0.5 Hz without bipolar cell current injection (Baccus et al., 2008; Ölveczky et al., 2003).

Data analysis

For extracellular recordings, spike trains from individual ganglion cells were extracted from raw voltage traces by a semi-automated spike-sorting algorithm written in Igor (Wave Metrics; Pouzat et al., 2002). Although the ganglion cell layer contains some displaced amacrine cells as well, their action potentials are expected to be below the noise level of the multielectrode recordings and are attenuated further by signal filtering prior to spike sorting (Segev et al., 2004). The extracted spike timing data and intracellular data traces were then analyzed in Matlab (Mathworks). The significance level is 0.05 in all analyses except where noted otherwise.

Receptive field analysis

The spatio-temporal receptive fields of the recorded cells were estimated by reverse-correlation methods (Meister et al., 1994). Using the random flicker stimulus, we computed the response-weighted average of the stimulus waveform (0.4 s window; 0.01 s bin width), where the weight is the measured membrane voltage for bipolar cells (Figure 1A) or amacrine cells, and spike number for ganglion cells (Figure 1C, D). To characterize the receptive field structures, we computed two-dimensional Gaussian fits to the spatial receptive field at the peak latency. The location of the cell was then assigned to the center of that Gaussian profile (Figure 1B), and the size of the receptive field diameter was estimated as twice the mean standard deviation of the long and short axes (Figure 2C, D).

Cell-type classification

The five major classes of retinal neurons can be recognized unambiguously by online analysis. Within each class, cells show a wide range of anatomical and physiological properties (Awatramani and Slaughter, 2000; DeVries, 2000; Masland, 2012; Wu et al., 2000). In this study, the need for simultaneous recording prohibited a morphological analysis of individual neurons. Specifically, because we serially impaled multiple cells in each retina with sharp electrodes, we failed to identify the exact target cells after recordings. We thus focused on visual response properties for cell type classification (Figure S3; see also Geffen et al., 2009). First we performed a principal component analysis on the temporal filters derived from receptive field analysis of all bipolar or ganglion cells (Figure S3A and D, respectively). The first two principal components (PC1 and PC2) were largely sufficient to fit all the waveform shapes, accounting for 78% of the total variance

for bipolar cells (Figure S3B) and 77% for ganglion cells (Figure S3E). Each waveform is a point in the two-dimensional space spanned by PC1 and PC2, and we characterized its shape by the angle around the origin, $\theta \in (-\pi, \pi]$, with $\theta = 0$ for PC1 and $\theta = \pi/2$ for PC2. Finally, based on this angle θ, we grouped bipolar and ganglion cells into four subtypes each. For bipolar cells, the boundaries for the four subtypes (Slow OFF, Fast OFF, Slow ON, and Fast ON bipolar cell types) were set to be $-3\pi/4$, 0, $\pi/4$, and $\pi/2$ (Figure S3C). For ganglion cells, the boundaries were set to be $-2\pi/3$, $-\pi/4$, 0, and $\pi/3$, corresponding to the Slow OFF, Fast OFF, ON/OFF, and ON ganglion cell types, respectively (Figure S3F).

For the salamander retina, cells in this feature space tend to form a continuum rather than breaking naturally into discrete clusters (Figure S3B, E; Segev et al., 2006). Any of the subtypes we defined might thus contain several cell types if classified by different criteria. Here we made a finer cell-type classification in the following three ways. Note that ON cell types were excluded from this refined analysis due to scarcity of the data.

1. We subdivided each of the bipolar and ganglion cell types based on the receptive field size (boundary at the median; Figure S3D and H, respectively).

2. We classified ganglion cells into direction selective and non-selective types (Vaney et al., 2012). Ganglion cell direction selectivity was estimated from the spatiotemporal receptive field, $R(\mathbf{x}, t)$, where $\mathbf{x}$ and t represent space and time, respectively. Specifically, we first Fourier transformed $R(\mathbf{x}, t)$ to represent the receptive field in the frequency domain: $\widehat{R}(\boldsymbol{\omega}, \xi) = \mathcal{F}[R(\mathbf{x}, t)]$. Here $\boldsymbol{\omega}$ and ξ are spatial and temporal frequency, respectively; and $\mathcal{F}[\cdot]$ is the three-dimensional Fourier transform. We then identified the frequencies $(\boldsymbol{\omega}_{\text{max}} \neq 0, \xi_{\text{max}} \neq 0)$ where the amplitude spectrum $|\widehat{R}(\boldsymbol{\omega}, \xi)|$ was maximal, and introduced a direction-selectivity (DS) index as follows:

$$\text{DS index} = \frac{|\widehat{R}(\boldsymbol{\omega}_{\text{max}}, \xi_{\text{max}})| - |\widehat{R}(\boldsymbol{\omega}_{\text{max}}, -\xi_{\text{max}})|}{|\widehat{R}(\boldsymbol{\omega}_{\text{max}}, \xi_{\text{max}})| + |\widehat{R}(\boldsymbol{\omega}_{\text{max}}, -\xi_{\text{max}})|}. \tag{S1}$$

   Note that $|\widehat{R}(\boldsymbol{\omega}_{\text{max}}, \xi_{\text{max}})|$ and $|\widehat{R}(\boldsymbol{\omega}_{\text{max}}, -\xi_{\text{max}})|$ represent the linear estimate of the ganglion cell response to a grating stimulus moving in preferred and null direction, respectively. We classified a ganglion cell as direction selective if $|\widehat{R}(\boldsymbol{\omega}_{\text{max}}, \xi_{\text{max}})| \geq 2|\widehat{R}(\boldsymbol{\omega}_{\text{max}}, -\xi_{\text{max}})|$, that is, DS index $\geq 1/3$ (Figure S3I).

3. We sorted ganglion cells into object motion sensitive and non-sensitive groups (Baccus et al., 2008; Ölveczky et al., 2003). In a subset of our recordings, we presented a grating stimulus and shifted either the entire grating rigidly ("global") or the center and surround regions at different times ("differential"). Based on the firing responses to these two stimuli, r_{global} and r_{diff}, respectively, we then introduced an index for the object motion sensitivity (OMS):

$$\text{OMS index} = \frac{r_{\text{diff}} - r_{\text{global}}}{r_{\text{diff}} + r_{\text{global}}}. \tag{S2}$$

Because the circular center region (1 mm diameter) was centered at the impaled bipolar cells but not at individual ganglion cells, here we excluded those ganglion cells outside the anatomically expected range of monosynaptic transmission (0.35 mm; Pang et al., 2004; Wu et al., 2000; Zhang and Wu, 2009, 2010). We classified a ganglion cell as object motion sensitive if $r_{\text{diff}} \geq 4r_{\text{global}}$, that is, OMS index ≥ 0.6 (Figure S3J).

Projective field analysis

We used the following methods to identify the projection from upstream bipolar (or amacrine) cells to downstream ganglion cells and estimate the projective field. For each target neuron, we measured the strength of the projection and its kinetics. First, we computed the peri-stimulus time histogram (0.1 s bin width) of ganglion cell spiking activity while injecting current into a bipolar (or amacrine) cell intracellularly. For those ganglion cells that showed significantly different firing rates from their baseline activity r_{base} (1 s period before the onset of the current injection) in at least one bin during the current injection periods (two-tailed *t*-test with Bonferroni correction), we calculated the average firing rates across trials for the 1-s periods of bipolar (or amacrine) cell depolarization and hyperpolarization: r_{dep} and r_{hyp}, respectively. If the net evoked firing rate, $r = r_{\text{dep}} - r_{\text{hyp}}$, was significantly above or below zero, then we considered that the bipolar (or amacrine) cell carried sign-preserving or sign-inverting signals to the ganglion cell, respectively. Confidence intervals were estimated by bootstrap resampling methods over trials (10,000 repeats).

The noise floor was estimated by resampling methods where spike timings were randomly shifted to neutralize the temporal correlation to the onset of the current injection, followed by the same significance

tests described above. For each cell, we repeated this procedure 1,000 times, and took the average over the population to calculate the level of false positives in the analysis (e.g., $p = 0.006$ in Figure 3B).

The spatial extent of bipolar (or amacrine) cell signals was then estimated by the probability of having a significant projection above the noise floor as a function of distance (Z-test with Bonferroni correction; Figures 3, 4, and 7). This is a conservative estimate of connection probability, because statistical significance is limited by the finite data length, and because we measured spiking activity of ganglion cells but not their subthreshold responses. Nevertheless, the estimate is not biased and thus supports a statistical comparison (χ^2-test) across different cell types (Figure 6) or different conditions (Figures 4 and 7). The dominance of OFF cell types over ON types in the salamander retina (Segev et al., 2006; Vallerga and Usai, 1986), however, poses a limitation on the analysis across distinct cell types (Figures 5, 6, and S3). For example, we rarely observed significant projection from ON bipolar cells to ON ganglion cells (1 out of 44 cell pairs; Figure 5A, B). This was significantly less than the projection between OFF bipolar cells and ON ganglion cells (28 out of 149 cell pairs; $p = 0.007$, proportion test), but not between ON bipolar cells and ON/OFF ganglion cells (34 out of 418 cell pairs; $p > 0.16$). The scarcity of the projection between ON cell types is thus most likely due to lack of data, but not the absence of the projections.

To quantify the projection strength of individual cell pairs regardless of the significance from the above analysis, we used the following definition (Asari and Meister, 2012):

$$\text{Projection strength} = \frac{\text{Net evoked firing rate}}{\text{Pooled standard deviation}} = \frac{r_{\text{dep}} - r_{\text{hyp}}}{\sqrt{(s_{\text{dep}}^2 + s_{\text{hyp}}^2)/2}}, \qquad \text{(2; revisited)}$$

where s_{dep} and s_{hyp} are the standard deviation of the ganglion cell firing rates across trials of bipolar (or amacrine) cell depolarization and hyperpolarization, respectively. This standardized measure does not depend on the data length (number of trials), unlike the p-values in the significance tests. The observed projection strength or its change were not correlated with the baseline firing property of ganglion cells or its change under different conditions (Figures S1, S2, and S5). Confidence intervals were estimated by the bootstrap resampling methods over trials (10,000 repeats; e.g., Figure 2A).

We used a Gaussian fit $g(x)$ to characterize the projection strength as a function of distance x between cell pairs:

$$g(x) = a \exp\left[-\frac{x^2}{2b^2}\right], \qquad \text{(S3)}$$

where a and b are the amplitude and radius of the Gaussian envelope, respectively (Figure 2). The projective field diameter was measured as $2b$.

To characterize the projection dynamics, we first fitted the following unimodal function $f(t)$ to the peri-stimulus time histogram of ganglion cell responses under current stimulation of a bipolar or amacrine cell (Asari and Meister, 2012):

$$f(t) = \alpha t^{\beta} \exp\left[-\frac{t}{\gamma}\right] + r_{\text{base}}, \tag{S4}$$

where α, β, and γ denote the free parameters, and t (> 0) indicates the time after the onset of current injection. The peak latency was then computed as $t_{\text{peak}} = \beta\gamma$ and the peak evoked firing rate as $r_{\text{peak}} = f(t_{\text{peak}}) - r_{\text{base}}$. For those projections with $r_{\text{peak}} > 1$ spike/s, we calculated the pairwise correlation coefficients among t_{peak}, the projection strength, and the distance between the cells (Figures 3 and 6) with p-values for testing the hypothesis of no correlation.

Linear analysis of receptive and projective fields

In Figure 2E, the measured bipolar and ganglion cell receptive fields were computed by averaging the spatial filters over the respective population. The measured bipolar cell projective field was acquired by pooling the projection profile (e.g., Figure 2A) over all bipolar cells and smoothing by local linear regression spanning 20% of the data. From Eq.(1), the predicted ganglion cell receptive field was then obtained by the linear convolution of the measured bipolar cell receptive and projective fields. Vice versa, the predicted bipolar cell projective field was obtained by deconvolving the measured ganglion cell receptive field with the measured bipolar cell receptive field.

Supplemental references

Asari, H. and Meister, M. (2012). Divergence of visual channels in the inner retina. Nat Neurosci, 15, 1581–1589.

Awatramani, G. B. and Slaughter, M. M. (2000). Origin of transient and sustained responses in ganglion cells of the retina. J Neurosci, 20, 7087–7095.

Baccus, S. A. and Meister, M. (2002). Fast and slow contrast adaptation in retinal circuitry. Neuron, 36, 909–919.

Baccus, S. A., Ölveczky, B. P., Manu, M., and Meister, M. (2008). A retinal circuit that computes object motion. J Neurosci, 28, 6807–6817.

Cook, P. B., Lukasiewicz, P. D., and McReynolds, J. S. (2000). $GABA_c$ receptors control adaptive changes in a glycinergic inhibitory pathway in salamander retina. J Neurosci, 20, 806–812.

DeVries, S. H. (2000). Bipolar cells use kainate and AMPA receptors to filter visual information into separate channels. Neuron, 28, 847–856.

Geffen, M. N., Broome, B. M., Laurent, G., and Meister, M. (2009). Neural encoding of rapidly fluctuating odors. Neuron, 61, 570–586.

Geffen, M. N., de Vries, S. E. J., and Meister, M. (2007). Retinal ganglion cells can rapidly change polarity from Off to On. PLoS Biol, 5, e65.

Masland, R. H. (2012). The neuronal organization of the retina. Neuron, 76, 266–280.

Meister, M., Pine, J., and Baylor, D. A. (1994). Multi-neuronal signals from the retina: acquisition and analysis. J Neurosci Methods, 51, 95–106.

Ölveczky, B. P., Baccus, S. A., and Meister, M. (2003). Segregation of object and background motion in the retina. Nature, 423, 401–408.

Pang, J.-J., Gao, F., and Wu, S. M. (2004). Stratum-by-stratum projection of light response attributes by retinal bipolar cells of *Ambystoma*. J Physiol, 558, 249–262.

Pouzat, C., Mazor, O., and Laurent, G. (2002). Using noise signature to optimize spike-sorting and to assess neuronal classification quality. J Neurosci Methods, 122, 43–57.

Segev, R., Goodhouse, J., Puchalla, J., and Berry, M. J. (2004). Recording spikes from a large fraction of the ganglion cells in a retinal patch. Nat Neurosci, 7, 1154–1161.

Segev, R., Puchalla, J., and Berry, M. J. (2006). Functional organization of ganglion cells in the salamander retina. J Neurophysiol, 95, 2277–2292.

Vallerga, S. and Usai, C. (1986). Relation between light responses and dendritic branching in the salamander ganglion cells. Exp Biol, 45, 81–90.

Vaney, D. I., Sivyer, B., and Taylor, W. R. (2012). Direction selectivity in the retina: symmetry and asymmetry in structure and function. Nat Rev Neurosci, 13, 194–208.

Veruki, M. L. and Hartveit, E. (2009). Meclofenamic acid blocks electrical synapses of retinal AII amacrine and on-cone bipolar cells. J Neurophysiol, 101, 2339–2347.

Wu, S. M., Gao, F., and Maple, B. R. (2000). Functional architecture of synapses in the inner retina: segregation of visual signals by stratification of bipolar cell axon terminals. J Neurosci, 20, 4462–4470.

Zhang, A.-J. and Wu, S. M. (2009). Receptive fields of retinal bipolar cells are mediated by heterogeneous synaptic circuitry. J Neurosci, 29, 789–797.

Zhang, A.-J. and Wu, S. M. (2010). Responses and receptive fields of amacrine cells and ganglion cells in the salamander retina. Vision Res, 50, 614–622.